Nuclear Physics A549 (1992) 180–196
North-Holland

NUCLEAR PHYSICS A

Transition charge densities of low-lying collective states in ^{196}Pt from inelastic electron scattering

V.Yu. Ponomarev[a,b,1], W.T.A. Borghols[b,c,2], S.A. Fayans[d], M.N. Harakeh[a], C.W. de Jager[c], J.B. van der Laan[c], A.P. Platonov[d], H. de Vries[c] and S.Y. van der Werf[c]

[a] *Faculteit Natuurkunde en Sterrenkunde, Vrije Universiteit, de Boelelaan 1081, 1081 HV Amsterdam, The Netherlands*

[b] *Kernfysisch Versneller Instituut, Zernikelaan 25, 9747 AA Groningen, The Netherlands*

[c] *National Institute for Nuclear Physics and High-Energy Physics, Section K, P.O. Box 41882, 1009 DB Amsterdam, The Netherlands*

[d] *I.V. Kurchatov Institute of Atomic Energy, Moscow 123182, Russian Federation*

Received 18 March 1992

Abstract: Differential cross sections for levels in the excitation-energy range from 0 to 3.0 MeV in ^{196}Pt have been measured by inelastic electron scattering in a momentum-transfer range up to 2.5 fm^{-1}. The ground-state charge density and the transition charge densities of nine low-lying collective levels have been extracted in a Fourier-Bessel analysis of these data. The densities are compared with those obtained from microscopic calculations within the quasiparticle phonon model, using the single-particle basis obtained from a density functional approach. Satisfactory agreement has been obtained, in spite of the complicated structure of ^{196}Pt.

E | NUCLEAR REACTIONS ^{196}Pt(e, e'), E = 90–334 MeV; measured spectra, longitudinal form factors, ^{196}Pt levels, Fourier-Bessel analysis, deduced transition charge densities, J, π, $B(\lambda)$. Compared to microscopic quasiparticle phonon model.

1. Introduction

The use of high-resolution spectrometers in inelastic electron scattering experiments makes it possible to investigate in detail the properties of low-lying states up to 3–4 MeV excitation energy, depending on the level density of the isotope being studied. The well-known mechanism of the (e, e') reaction allows the extraction of the transition charge and current densities of these states in a model-independent way. The transition densities present a sensitive test for different theoretical approaches as they carry detailed information on the radial structure of nuclei in

[1] Permanent address: Laboratory of Theoretical Physics, Joint Institute for Nuclear Research, Dubna, Head Post Office, P.O. Box 79, Moscow, Russian Federation.

[2] Present address: Gasunie, Groningen, The Netherlands.

their excited states, whereas integral characteristics such as the transition rates, i.e. $B(E\lambda)$ or $B(M\lambda)$ values, are mainly sensitive to the behaviour of the transition densities in the tail of the nuclear density.

During the past ten years such experiments have been performed at various electron accelerator facilities. This paper belongs to a series of papers presenting the results of these experiments in various mass regions: $A \simeq 90$ [refs. [1,2])], the tin isotopes [3]), $A \simeq 140$ [refs. [4-12])], $A \simeq 190$ [ref. [13])] and $A \simeq 208$ [ref. [14])]. Spherical isotopes are simpler to deal with because of the moderate level density at low excitation energy allowing the resolution of many excited levels, but deformed nuclei such as ^{150}Nd [refs. [7-9])] and ^{152}Sm [ref. [12])] have been investigated as well. ^{196}Pt is considered to be a γ-soft transitional nucleus with a small triaxial deformation in its ground state. It would be interesting to compare the results for this isotope with those for another transitional nucleus ^{146}Nd in which it has been found from recent similar (e, e′) experiments [6,9]) that the lowest excited states retain the ground-state static deformation while the higher excitations can be considered as excited states of a spherical nucleus.

In a preliminary report on the ^{196}Pt(e, e′) measurements [15]) the hexadecapole states have been analysed in the framework of the interacting boson approximation (IBA). In the present paper the transition charge densities for all low-lying states observed in this experiment in the excitation energy range of 0 to 3 MeV are presented together with the results of microscopic calculations within the quasiparticle phonon model (QPM) [refs. [16-19])] and the self-consistent finite Fermi system theory (FFS) [refs. [20-22])]. The latter theory is based on the density functional approach. These two approaches have been successfully applied in the interpretation of results from (e, e′) measurements for several of the spherical isotopes mentioned above [2-5,9-11]). Such calculations are much more complicated for transitional nuclei with strong anharmonic effects and *a priori* we do not expect to get the same quality of description as for spherical cases. However, the reasonable description of the ^{146}Nd(e, e′) data, obtained at least for several excited states in the spherical picture [6]), encouraged us to apply the same approach also in case of ^{196}Pt.

The properties of low-lying states in ^{196}Pt have also been investigated in experiments on inelastic scattering of protons [23]), and α-particles [24]), the (d, ^{3}He) reaction [25,26]), the two-nucleon transfer reaction (t, p) [ref. [27])], an (n, γ) study [28]), the (d, pnγ) reaction [29]) and in Coulomb excitation by heavy ions [30]). New experimental information from (e, e′) scattering will complement this available information.

2. Experimental set-up and data analysis

The experiment was performed with the high-resolution QDD spectrometer in the EMIN facility at NIKHEF-K [31]). The target was a self-supporting foil, enriched to 99% in ^{196}Pt, of thickness 7.1 mg/cm^2. Spectra were taken at energies between 90 and 334 MeV at scattering angles between 35° and 85°, thus covering an effective

momentum-transfer ($q_{\rm eff}$) range between 0.36 and 2.43 fm^{-1}. With the use of the energy-loss technique, in which the dispersion in the beam at the target is matched to the dispersion of the spectrometer, and after application of corrections for kinematic broadening and spectrometer aberrations, a momentum resolution of around 8×10^{-5} was obtained.

Three additional data points were taken at a scattering angle of 154° in order to estimate the relative importance of the transverse contribution to the cross section. From these measurements no indication of transverse strength was found within the error bars of the data. Cross sections were derived from peak areas which were extracted from the measured spectra with the line-shape fitting program ALLFIT [32]). For calibration purposes measurements were also performed on a ^{12}C target and a BN target of natural composition. Uncertainties in the detector efficiencies, target alignment and solid angle were corrected for by the aforementioned calibration runs on ^{12}C. The energy calibration was obtained from an analysis of several elastic and inelastic peaks in ^{196}Pt, ^{12}C and B and N isotopes.

The ground-state charge distribution of ^{196}Pt was extracted using a standard Fourier-Bessel analysis with the computer code MEFIT [33]). For 9 out of the 26 levels observed at excitation energies up to 3 MeV, transition charge densities were extracted via a Fourier-Bessel analysis with the program FOUBES [34]). A cut-off radius of 12 fm was assumed. An exponential fall-off was assumed for the form factor above 2.5 fm^{-1}. Small unphysical oscillations in the tail of the distribution were removed by the application of a so-called tail bias, which forces the density distribution to follow an exponentially decreasing shape beyond a certain radius. Whenever a $B(E\lambda)$ value was known from the literature this value was used as an extra data point in the analysis.

3. Microscopic approaches for the description of properties of low-lying states

In this section two theoretical approaches used to interpret the experimental data, the self-consistent FFS and the QPM theories, are briefly outlined. Both were successful in describing transition charge densities of low-lying states in previous experiments on the half-magic nuclei ^{118}Sn [ref. [3])], ^{140}Ce [ref. [11])] and ^{142}Nd [refs. [4,5])], the non-magic spherical nuclei ^{86}Sr [ref. [2])] and ^{142}Ce [ref. [10])] and the transitional nucleus ^{146}Nd [ref. [6])]. In this paper, these approaches, developed for the description of spherical nuclei, are tested for excited states in transitional nuclei. We shall try to combine the advantages of both the FFS and QPM approaches in an attempt to achieve a good microscopic description for ^{196}Pt. In the following the main ideas of these approaches will be pointed out.

In the present paper a version of the FFS is used which allows a self-consistent description of both the ground state and the excited collective states. For this purpose the density functional approach was used in the form close to that suggested in ref. [22]). The corresponding energy density as a function of r is represented as a sum

of four terms:

$$\varepsilon_{\rm int}(r) = \varepsilon_{\rm main}(r) + \varepsilon_{\rm Coul}(r) + \varepsilon_{\rm sl}(r) + \varepsilon_{\rm pair}(r)\,. \tag{1}$$

The main term is given by

$$\varepsilon_{\rm main}(r) = \tfrac{2}{3}\varepsilon_{\rm F}^0\rho_0(r)[a_+^{\rm v}x_+(r)^2 f_+^{\rm v}(r) + a_-^{\rm v}x_-(r)^2 f_-^{\rm v}(r) + a_+^{\rm s}x_+(r)f_+^{\rm s}(r)\widetilde{f_+^{\rm s}x_+}(r) + a_-^{\rm s}x_-(r)f_-^{\rm s}(r)f_-^{\rm s}x_-(r)]\,. \tag{2}$$

Here $x_\pm(r) = [\rho_{\rm n}(r) \pm \rho_{\rm p}(r)]/2\rho_0(r)$, $\rho_{\rm n(p)}(r)$ is the neutron (proton) density, $2\rho_0(r)$ is the equilibrium nuclear-matter density ($N = Z$), $\varepsilon_{\rm F}^0$ is the nuclear-matter Fermi energy and the functions $f_\pm^{\rm v}(r)$ and $f_\pm^{\rm s}x_\pm(r)$ are given by

$$f_\pm^{\rm v}(r) = \frac{1 - h_{1\pm}^{\rm v}x_+(r)}{1 + h_{2\pm}^{\rm v}x_+(r)}, \qquad f_\pm^{\rm s}(r) = \frac{1}{1 + h_\pm^{\rm s}x_+(r)}, \tag{3}$$

$$\widetilde{f_\pm^{\rm s}x_+}(r) = \int D(r - r')f_\pm^{\rm s}(r')x_\pm(r')\,{\rm d}r'\,, \tag{4}$$

with

$$D(r - r') = \delta(r - r') - \frac{1}{4\pi R^2|r - r'|}\exp\left(\frac{-|r - r'|}{R}\right). \tag{5}$$

The first two terms of $\varepsilon_{\rm main}(r)$ are the contributions of the volume isoscalar and isovector interaction energy and the last two terms are generated by the surface finite-range density-dependent forces.

The usual form including the exchange part in the Slater approximation is taken for the energy density of the Coulomb interaction $\varepsilon_{\rm Coul}(r)$. The term $\varepsilon_{\rm sl}(r)$ comes from spin-orbit and velocity spin-dependent interactions. The term $\varepsilon_{\rm pair}(r)$ is the pairing-energy density generated by simple δ-function effective particle-particle forces.

The parameters of the density functional ($a_\pm^{\rm v}$, $a_\pm^{\rm s}$, $h_{1,2\pm}^{\rm v}$, $h_\pm^{\rm s}$, etc.) were chosen by fitting binding energies, charge distributions and single-particle level spectra for a number of nuclei, both magic (^{40}Ca, ^{48}Ca, ^{208}Pb) and non-magic (^{90}Zr, ^{146}Gd, tin and lead even-even isotopes). The results of these calculations will be published elsewhere [35]). The above functional is described in more detail in ref. [2]) where a basic set of its parameters deduced from this fitting procedure, hereafter referred to as set I, is also given.

The FFS equations for one-phonon excitations were solved in a mixed coordinate-shell configuration, the (r, λ) representation. A self-consistent single-particle basis and an effective interaction, obtained as a second variational derivative of this functional with respect to the nucleon densities (obtained with this functional), were used in which the particle-hole continuum was taken fully into account as in refs. [10,21]). The main advantage of this approach is that the FFS theory employs a realistic form of the residual interaction between quasiparticles with a single fixed

set of parameters for different nuclei. On the other hand, the most straightforward way to take into account the interplay between the various modes of excitation is to use the QPM, though in this approach a more schematic form of the residual interaction is used with parameters adjusted to the experimental data for each nucleus. Self-consistent consideration of such mixing of one- and two-phonon configurations within the FFS theory will be described in a separate paper.

The QPM deals with an effective nuclear hamiltonian which includes an average field for neutrons and protons, a pairing interaction and a multipole residual interaction of separable form with the Bohr-Mottelson radial dependence. In previous papers [see e.g. refs. [5,10])] the QPM calculations have been performed with a Woods-Saxon potential for the average field and a monopole-pairing interaction with a constant matrix element (one for neutrons and one for protons) adjusted to reproduce the pairing energies of neighbouring nuclei. In this paper we use the quasiparticle spectrum and single-particle wave functions obtained in the FFS calculation for the ground state. The QPM equations for excited states are solved in the shell configuration (λ-)space, which essentially simplifies the calculation of the interaction between different phonon configurations. A quasibound-state approximation is used instead of an exact treatment of the continuum. Earlier calculations in heavy nuclei showed that this approximation is suitable for low-spin states and that the collectivity of low-lying collective excitations is well reproduced without introducing effective charges. In the present calculation 34 single-particle levels for neutrons and 32 for protons are used, of which 18 are quasibound.

Excited states of even-even nuclei are considered in the QPM as a combination of one-, two-, ... phonon configurations built upon the wave function of the ground state $\Psi_{\text{g.s.}}$, which is treated as the phonon vacuum. The wave function for the νth excited state with angular momentum λ and projection μ is given by

$$\Psi_\nu(\lambda\mu) = \Bigg(\sum_i R_i(\lambda\nu) Q^+_{\lambda\mu i} + \sum_{LIL'I'} P^{LI}_{L'I'}(\lambda\nu) [Q^+_{LMI} Q^+_{L'M'I'}]_{\lambda\mu} + \sum_{LIL'I'} \sum_{\lambda' L''I''} T^{\lambda' L''I''}_{LIL'I'}(\lambda\nu) [[Q^+_{LMI} Q^+_{L'M'I'}]_{\lambda'\mu'} Q^+_{L''M''L''}]_{\lambda\mu} + \cdots \Bigg) \Psi_{\text{g.s.}}, \quad (6)$$

where

$$[Q^+_{LMI} Q^+_{L'M'I'}]_{\lambda\mu} \equiv \sum_{MM'} \langle LML'M' | \lambda\mu \rangle Q^+_{LMI} Q^+_{L'M'I'}. \quad (7)$$

Phonon operators $Q^+_{\lambda\mu i}$ with angular momentum λ and projection μ are constructed as a linear combination of pairs of quasiparticle creation α^+_{jm} and annihilation α_{jm} operators with the shell quantum numbers $jm \equiv |n, l, j, m\rangle$ as follows,

$$Q^+_{\lambda\mu i} = \tfrac{1}{2} \sum_{jj'}^{N,Z} \{ \psi^{\lambda i}_{jj'} [\alpha^+_{jm} \alpha^+_{j'm'}]_{\lambda\mu} + (-1)^{\lambda-\mu} \phi^{\lambda i}_{jj'} [\alpha_{jm} \alpha_{j'm'}]_{\lambda-\mu} \}. \quad (8)$$

Solving the RPA equations yields a set of one-phonon configurations for all λ^π, that are subsequently used to determine the wave functions of eq. (6), and the

coefficients $\psi_{jj'}^{\lambda i}$ and $\phi_{jj'}^{\lambda i}$ for the contribution of each two-quasiparticle $[\alpha_{jm}^{+}\alpha_{j'm'}^{+}]_{\lambda\mu}$ configuration in the structure of the ith λ^{π} one-phonon configuration. The hamiltonian is then diagonalized in the basis of these wave functions which yields the set of equations for eigenvalues of states of eq. (6). By solving these equations the spectrum of excited states and the contributions of one-, two-, ... phonon configurations [i.e. the coefficients $R_i(\lambda\nu)$, $P_{LI}^{L'I'}(\lambda\nu)$ and $T_{LIL'I'}^{\lambda'L''I''}(\lambda\nu)$] to the structure of the νth λ^{π} state are obtained. The transition charge density of the excited state (6) is a similar mixture of the one-phonon configurations $\rho_{\lambda i}(r)$ and the two-phonon configurations $\rho_{[LI\times L'I']\lambda}(r)$ densities:

$$\rho_{\lambda\nu}(r)=\sum_i R_i(\lambda\nu)\rho_{\lambda i}(r)+\sum_{LIL'I'} P_{LI}^{L'I'}(\lambda\nu)\rho_{[LI+L'I']_\lambda}(r)\,. \tag{9}$$

The explicit expressions for $\rho_{\lambda i}(r)$ and $\rho_{[LI\times L'I']_\lambda}(r)$ as well as a more detailed description of the QPM application to calculations of transition densities of low-lying states can be found in refs. [5,9,10]).

As mentioned above, in the framework presented here the QPM uses the Bohr-Mottelson residual multipole force and thus a few more parameters, i.e. the strength parameters of the residual interaction $\kappa_{0,1}^{\lambda\pi}$, are present in the QPM calculations than in the FFS ones. Based on previous experience [17]) the ratio between the isovector $\kappa_1^{\lambda\pi}$ and the isoscalar $\kappa_0^{\lambda\pi}$ strength parameters has been fixed to a value of -1.2. For $\lambda>4$ excitations we used $\kappa_0^{\lambda\pi}=\kappa_0^{2^+}$ for positive-parity states and $\kappa_0^{\lambda\pi}=\kappa_0^{3}$ for negative-parity states. Thus, three more parameters $\kappa_0^{2^+}$, κ_0^{3} and $\kappa_0^{4^+}$ have been adjusted to reasonably reproduce the positions and collectivity of the first excited states of each multipolarity in calculations with the wave functions of eq. (6). In the actual calculations it is necessary to truncate the space of the phonon configurations taken into account in these wave functions. In the present calculations all one-phonon configurations up to an excitation energy of 3.5 MeV, two-phonon configurations up to 6.5 MeV and three-phonon configurations constructed from only the first collective phonons have been included.

4. Results

In addition to the present experiment a limited amount of data from electron scattering [13]) and muonic X-ray [36]) experiments is available for this nucleus. The ground-state charge density of ^{196}Pt, deduced from the present (e, e) measurement, is shown in fig. 1, together with the elastic form factor. The r.m.s. radius was determined to be 5.38(2) fm, in good agreement with the available (e, e) result of 5.370(3) fm. The result of the muonic X-ray experiment is only quoted in the form of an equivalent Barrett radius and cannot be compared directly to the present result. The ground-state densities calculated within the FFS with two sets of the density functional parameters are also presented in this figure for comparison. The first set of parameters (set I, solid line), also used in previous calculations [2,3,11]), is the standard one for the FFS adjusted to reproduce ground-state properties for

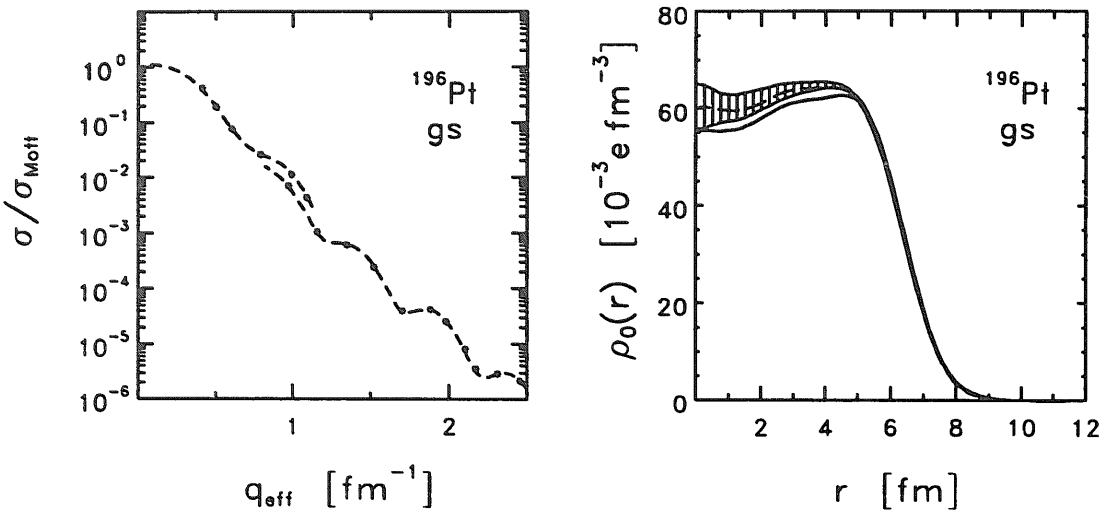

Fig. 1. The elastic form factor and the fit obtained in a Fourier-Bessel analysis (dashed curve) and the deduced experimental ground-state charge density of ^{196}Pt compared with the results of ground-state FFS calculations with two sets of parameters (set I: solid line; set II: long-dashed line; see text for further details).

different mass regions. The second one (set II, long-dashed line) is obtained especially for ^{196}Pt by changing the parameter r_0 of the basic set I [ref. [2])] from 1.135 to 1.120 fm. Both solid and long-dashed curves are practically identical in the surface region and very close to the experimental result. The solid curve in the interior region is close to the experimental data indicating that the FFS standard set of parameters can also be applied for ^{196}Pt. In the present paper we have used, however, both sets of parameters in the QPM calculations to check the stability of the results. The r.m.s. radius of the ground state resulting from calculations with sets I and II is 5.42 and 5.38 fm, respectively.

The inelastic-scattering data allowed the determination of the transition charge densities of nine excited states by means of a Fourier-Bessel analysis from the form factor data. The excitation energies and $B(E\lambda)$ values of these states are presented in table 1. Previous to our measurements, results for the 2_1^+, 3_1^- and 4_1^+ states in ^{196}Pt were obtained by (e, e') scattering. Our $B(E\lambda)$ values agree for the 2_1^+ and 3_1^- states and disagree with the $B(E4)$ value for the 4_1^+ state with those of ref. [13]). No form-factor data have been presented in ref. [13]), but the comparison of the extracted transition charge densities for the 4_1^+ states in ^{196}Pt and those of the other nuclei studied in the same reference indicate an inconsistency in the tail behaviour of these densities.

The experimental excitation energies and $B(E\lambda)$ values are compared in table 1 with the results of the QPM calculations with the wave functions of excited states, eq. (6), for two sets of the ground-state parameters (I and II). The only quadrupole transition observed in this experiment was the one corresponding to the first 2^+ state at $E_x = 0.356$ MeV. The $B(E2)$ value was determined to be $1.49 \times 10^4\ e^2\,\mathrm{fm}^4$.

TABLE 1

Excitation energies and $B(E\lambda)$ values of collective low-lying states in ^{196}Pt from the present experiment compared to results of the QPM calculations with two sets of parameters (see text)

λ^{π}_{ν}	Experiment		Calculations			
			set I		set II	
	E_x [MeV]	B(E$\lambda\uparrow$) [e^2 fm$^{2\lambda}$]	E_x [MeV]	$B(E\lambda\uparrow)$ [e^2 fm$^{2\lambda}$]	E_x [MeV]	$B(E\lambda\uparrow)$ [e^2 fm$^{2\lambda}$]
2^+_1	0.356	$1.49\times10^4\pm14\%$	0.25	6.16×10^3	0.31	6.85×10^3
4^+_1	0.877	$2.47\times10^6\pm22\%$	0.75	1.65×10^6	0.84	1.46×10^6
5^-_1	1.270	$2.04\times10^7\pm10\%$	1.20	1.43×10^8	1.33	1.21×10^8
4^+_2	1.293	$2.01\times10^6\pm20\%$	1.47	4.68×10^5	1.84	6.39×10^5
7^-_1	1.374		1.48	7.74×10^{10}	1.83	1.01×10^{11}
3^-_1	1.447	$1.16\times10^5\pm12\%$	2.08	1.03×10^5	2.17	8.94×10^4
4^+_3	1.887	$4.38\times10^6\pm29\%$	1.82	2.17×10^6	2.00	3.02×10^6
3^-_2	2.431	$8.68\times10^4\pm16\%$	2.94	5.20×10^4	3.21	2.82×10^4
3^-_3	2.638	$7.16\times10^4\pm18\%$	3.29	2.80×10^4	3.65	9.22×10^3

The form factor and the extracted transition charge density of this state are shown in fig. 2. The transition density is compared to the results of the QPM calculation obtained with the two sets of parameters: set I (solid line, hereafter also for set I calculations in all figures) and set II (long-dashed line, hereafter also for set II calculations in all figures) and the one-phonon approximation of the FFS calculation with set II (dot-dashed line). The FFS predicts the first 2^+ state at 0.47 MeV with a $B(E2)$ value of $2.23\times10^4\ e^2\,\mathrm{fm}^4$. Both approaches reproduce rather well the position of the experimental density maximum at 6.3 fm, the second maximum at 3.3 fm and the "minimum" at 1.4 fm. The amplitude of the surface peak and the $B(E2)$ value are overestimated by the FFS calculation and underestimated by the QPM calculation. The QPM calculation* yields as the structure of this state 81% of the first one-phonon 2^+ configuration and 11% of the two-phonon $[2^+_1\times4^+_1]_{2^+}$ configuration. Although $\kappa^{2^+}_0$ is a free parameter in the QPM, it was not possible to increase the collectivity of this state since a further increase in the $\kappa^{2^+}_0$ value leads to very large values for the matrix elements of the interaction between phonon configurations of different complexity (i.e. one- and two-phonon configurations) which results in a shift of the two-phonon configurations to unrealistically low energies.

To check the stability of the QPM results with respect to the truncation of the phonon basis we have performed a test calculation for 2^+ states in which all strong one- and two-phonon configurations up to the isoscalar giant-quadrupole resonance

* Since the values of the contributions of the different phonon configurations to the wave functions of excited states are slightly different in the calculations with the two sets of parameters, all values presented here correspond to the calculations with set I.

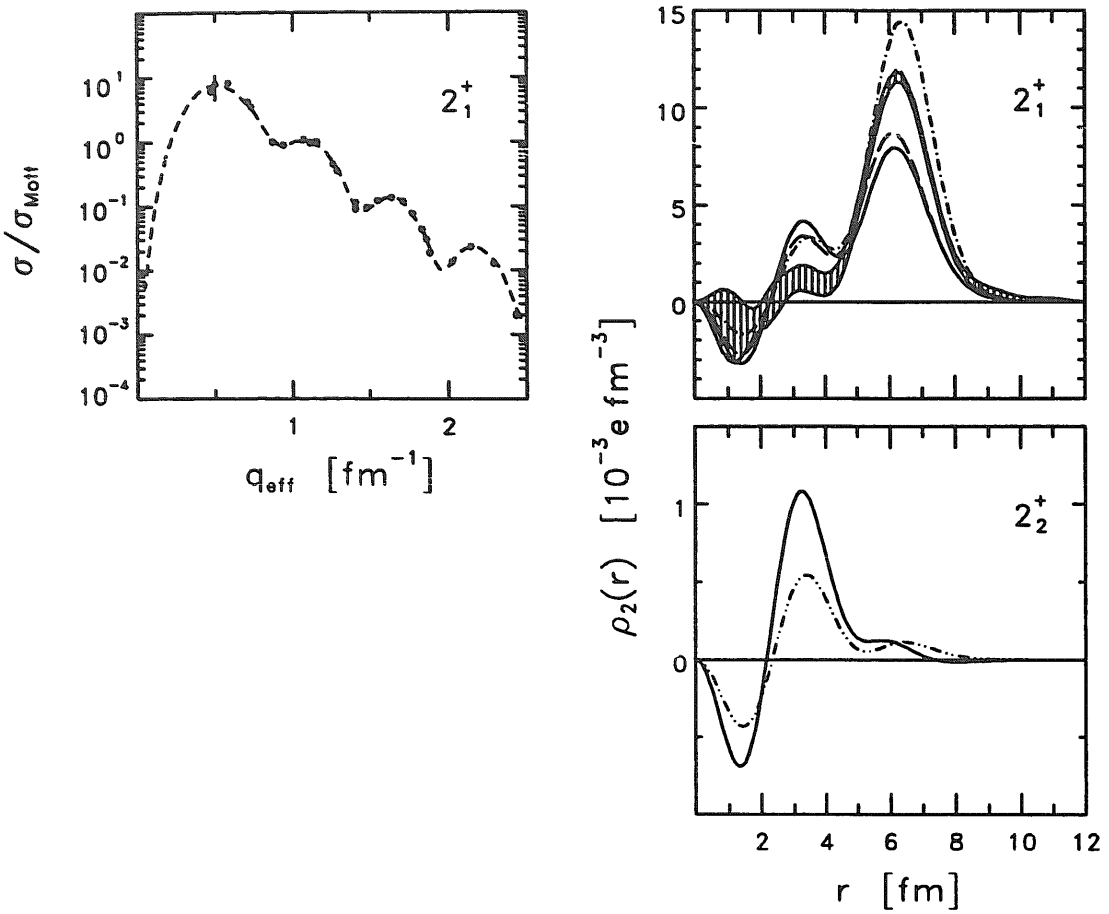

Fig. 2. Top: The inelastic form-factor data and the fit obtained in a Fourier-Bessel analysis (dashed line), and the deduced transition charge density of the 2_1^+ state compared to results of the QPM calculation with the wave function eq. (6) and two sets of parameters (set I: solid line; set II: long-dashed line; see text for further details) and to the one-phonon approximation of the FFS calculation (dot-dashed line). Bottom: The QPM transition charge density of the 2_2^+ state calculated with set I parameters (solid line) and the contribution of densities of one-phonon configurations (double dot-dashed line).

(GQR) region have been included. This calculation showed that the contribution of the GQR phonons in the framework of the QPM to the structure of low-lying states is negligibly small and can be omitted.

The QPM predicts ten 2^+ states in the energy region up to 3 MeV but all of them are very weak (the strongest one at 2.67 MeV has a B(E2) value of 60 e^2 fm^4) and therefore it is not surprising that no other 2^+ states have been observed in the present experiment. The structure of most of these states is rather complicated since eight one-phonon and several two-phonon 2^+ configurations are located in this region and the strength of most of these configurations is fragmented over several states. In fig. 2 we also present the transition charge density of the second 2^+ state predicted at 0.46 MeV. The main contribution (62%) to the structure of this state comes from the two-phonon $[2_1^+ \times 2_1^+]_{2^+}$ configuration with small admixtures of several one- and three-phonon configurations. This state corresponds to the known 2^+ state at 688 keV

which has a strong transition to the 2_1^+ state [37]). The experimental value of the ratio $B(\mathrm{E2}, 2_2^+ \to 2_1^+)/B(\mathrm{E2}, 2_1^+ \to 0_{\mathrm{g.s.}}^+)$, determined from the intensities of γ-decays of these levels under the assumption that the second 2^+ state decays to the 2_1^+ state predominantly by an E2 transition, is 1.4. The present calculation yields a value of 1.5 for this ratio. Although this state can be considered as a two-phonon state, the shape of its density is still determined by a small admixture of one-phonon configurations which is shown in the bottom of fig. 2 by a double dot-dashed line.

Three levels at 1.447, 2.431 and 2.638 MeV have been identified as 3^- levels in the present experiment. Their form factors and extracted transition charge densities are presented in fig. 3. The transition densities peak at 6.0, 6.3 and 6.5 fm, respectively, and the shapes of those of the first and the second 3^- levels are rather similar. In the QPM calculation the first three 3^- states appear to be a mixture of the first one-phonon 3^- configuration with low-lying two-phonon $[2_1^+ \times 3_1^-]_{3^-}$ and $[2_1^+ \times 5_1^-]_{3^-}$ configurations. The strength of the first one-phonon 3^- configuration is distributed over these states as 44%, 25% and 14%, respectively. Since the shape of the transition densities is determined mainly by the contribution from the one-phonon configuration, the calculated densities of the 3_1^- and 3_2^- states are very similar to each other. The shift of the maximum of the calculated density from 6.0 fm for the 3_1^- state to 6.1 fm for the 3_2^- state, though somewhat smaller than that of the experimental densities, appears as a result of the interference between densities of one-phonon 3_1^- and two-phonon $[2_1^+ \times 3_1^-]_{3^-}$ configurations. This leads to a small shift of the density maximum inwards for the 3_1^- state and outwards for the 3_2^- state.

The influence of the two-phonon configurations on the shape of the 3_3^- state in the QPM calculation is much stronger than for the $3_{1,2}^-$ states since the main contribution (71%) to the structure of this state comes from the two-phonon $[2_1^+ \times 5_1^-]_{3^-}$ configuration, which is shown in the left part of fig. 4. The interference with this two-phonon configuration results in a shift of the density maximum to 6.2 fm but nonetheless the agreement with the experimental density of this state can be considered to be only qualitative, especially for set II.

As in calculations for the Nd region [5,6,9]) the QPM overestimates the excitation energies of the 3^- states but the shape of the transition charge densities of the 3_1^- and 3_2^- states is reproduced rather well. Since the structure of the 3^- states is rather complicated, we do not present here the results obtained within the one-phonon approximation of the self-consistent FFS.

The structure of the low-lying 4^+ states in terms of phonon operators is very complicated, similar to that of the low-lying 2^+ states. There are four one-phonon 4^+ configurations in the energy region up to 3 MeV and they are all mixed in the wave functions of the 4^+ excited states. The essential feature of the 4^+ states is that the strength of the first one-phonon 4^+ configuration, which has the largest $B(\mathrm{E4})$ value, is fragmented over the three lowest states as 23%, 13% and 46% whereas the first one-phonon 2^+ configuration with the largest $B(\mathrm{E2})$ value is mainly concentrated in the 2_1^+ state. As a result three 4^+ states with large $B(\mathrm{E4})$ values appear in the

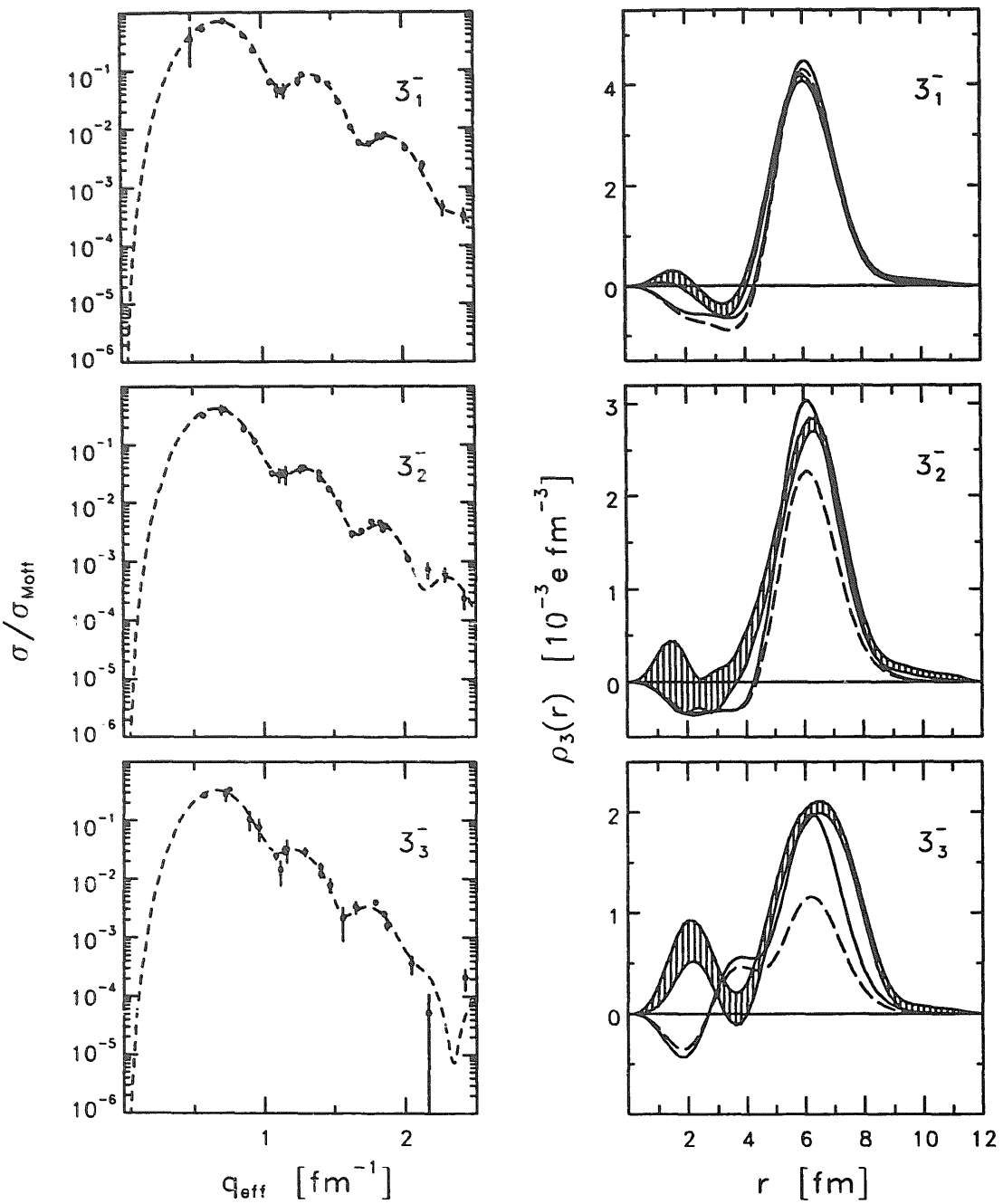

Fig. 3. The form factors and transition charge densities for 3^- states in ^{196}Pt. The curves have the same meaning as for the top part of fig. 2.

low-energy spectrum. They have been observed in the present experiment at 0.877, 1.293 and 1.887 MeV. The form factors and extracted transition charge densities of these states are presented in fig. 5. The experimental densities peak at 5.9, 6.4 and 6.2 fm, respectively. Similar to the 3^- states, the shift of the maximum of the transition density of the 4^+ states is explained in the QPM calculation as a result of admixture of two-phonon transition densities. The transition density of the first one-phonon

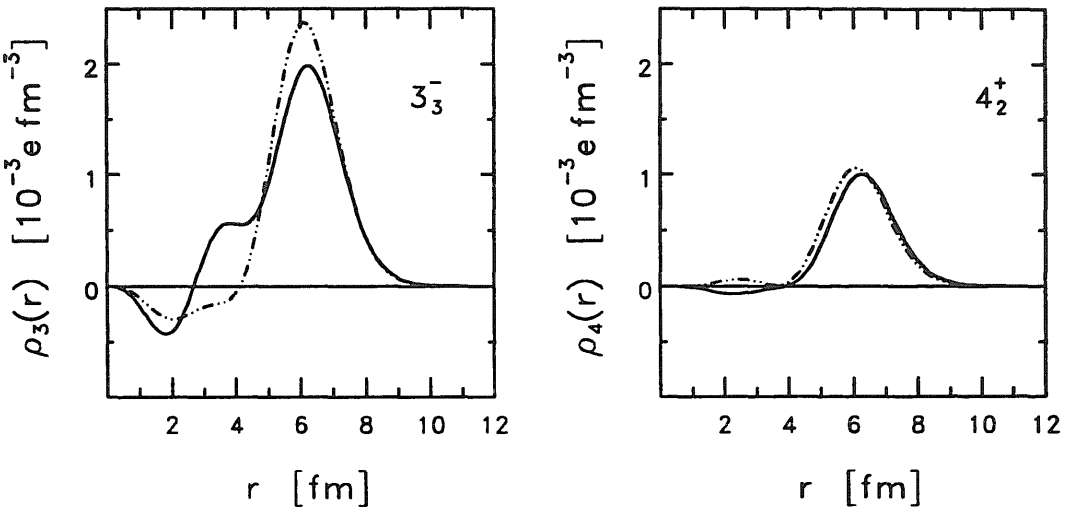

Fig. 4. The QPM transition charge densities for the 3_3^- and 4_2^+ states in ^{196}Pt. The curves have the same meaning as for the bottom part of fig. 2.

4^+ configuration has its maximum at 6.05 fm. The two-phonon $[2_1^+ \times 2_1^+]_{4^+}$ configuration contributes 46% to the wave function of the 4_1^+ state and shifts the density maximum to 5.95 fm, while a 10% contribution with an opposite sign to the structure of the 4_3^+ state produces a shift outwards to 6.1 fm. The shift of the maximum of the 4_2^+ transition density to 6.3 fm in the calculation is a result of a 54% contribution from the two-phonon $[2_1^+ \times 4_1^+]_{4^+}$ configuration to the wave function of this state; this is displayed in the right part of fig. 4.

Although the calculation somewhat underestimates the B(E4) values of all observed 4^+ states it reproduces rather well the B(E4) strength distribution. The QPM also predicts a 4^+ state at 2.64 MeV with a reasonably large B(E4) value of $1.9 \times 10^5\ e^2\,\mathrm{fm}^8$, which appears as a result of a 62% admixture of the fourth one-phonon 4^+ configuration with several other one- and two-phonon configurations. This state has not been observed in the present experiment, however. Other 4^+ states in the QPM calculation have very small B(E4) values.

The extracted transition charge densities of the 4_1^+ and 4_2^+ states have been used in ref. [15]) to determine the boson structure functions in an IBA-2 description of ^{196}Pt. As a result of the analysis of the form factor of the 4_3^+ state obtained with these IBA boson structure functions it has been claimed [15]) that the inclusion of the g-boson is needed in IBA. From the present microscopic calculation we can draw the conclusion that the one-phonon 4_1^+ and the two-phonon $[2_1^+ \times 4_1^+]_{4^+}$ configurations play a major role in determining the properties of low-lying 4^+ states supporting the claim by ref.[15]).

There is an open question concerning the existence of a 4^+ state at 1.537 MeV. The spin and parity assignments were suggested from a (d, pnγ) experiment [29]) as a result of the observed transitions $4_3^+(?) \rightarrow 3_1^+ \rightarrow 2_2^+$. Even if this state can be assigned 4^+, it must have a considerable contribution of many-phonon configurations in its

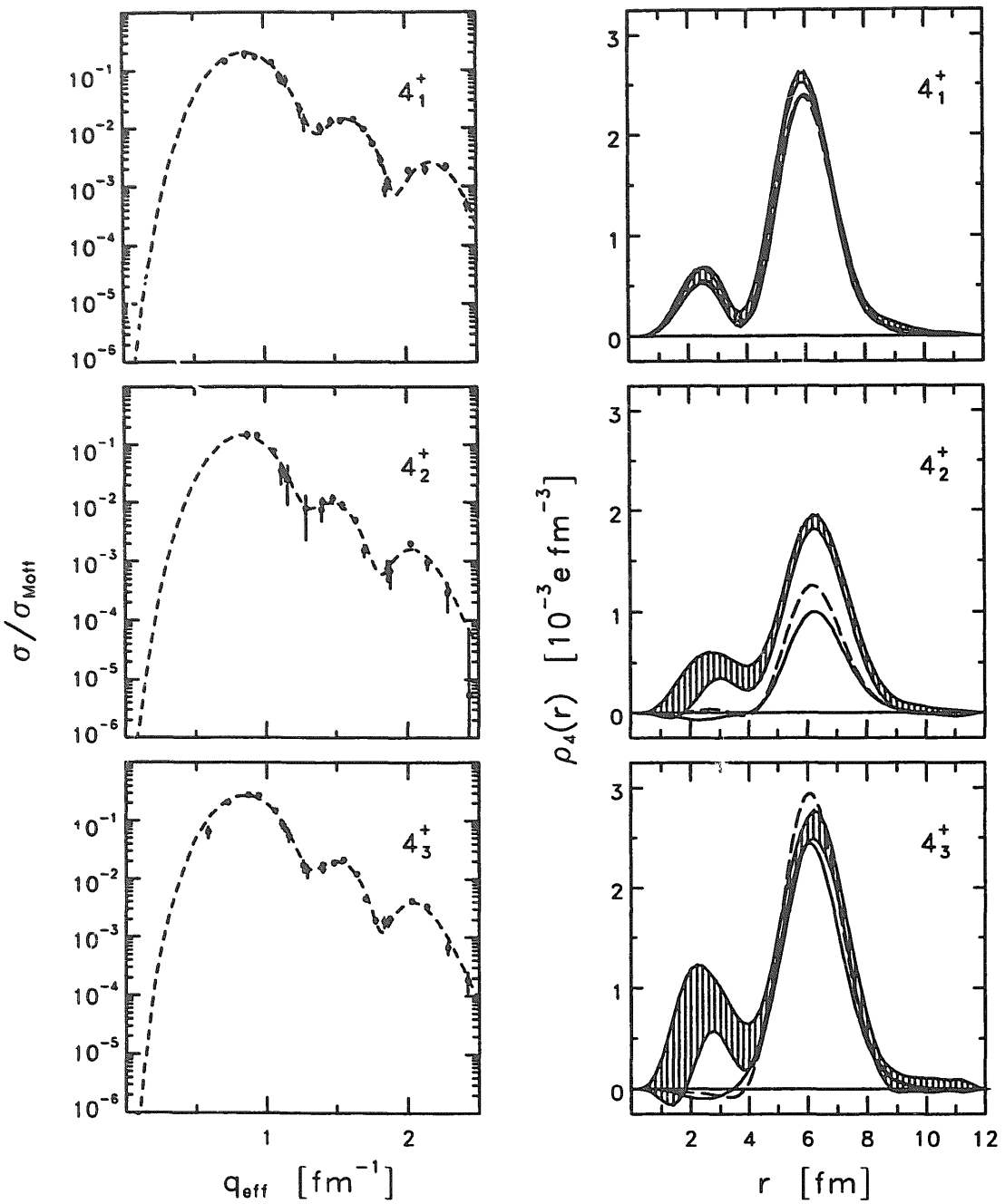

Fig. 5. The same as fig. 3 but for the 4^+ states in ^{196}Pt.

wave function to allow such a transition. These many-phonon configurations are not included in the present QPM calculation and such a state can therefore not be reproduced.

Only two states of high multipolarity have been identified in this experiment, the 5_1^- state at 1.270 MeV and the 7_1^- state at 1.374 MeV. Their form factors and extracted transition charge densities are presented in fig. 6. Both of these densities have surface

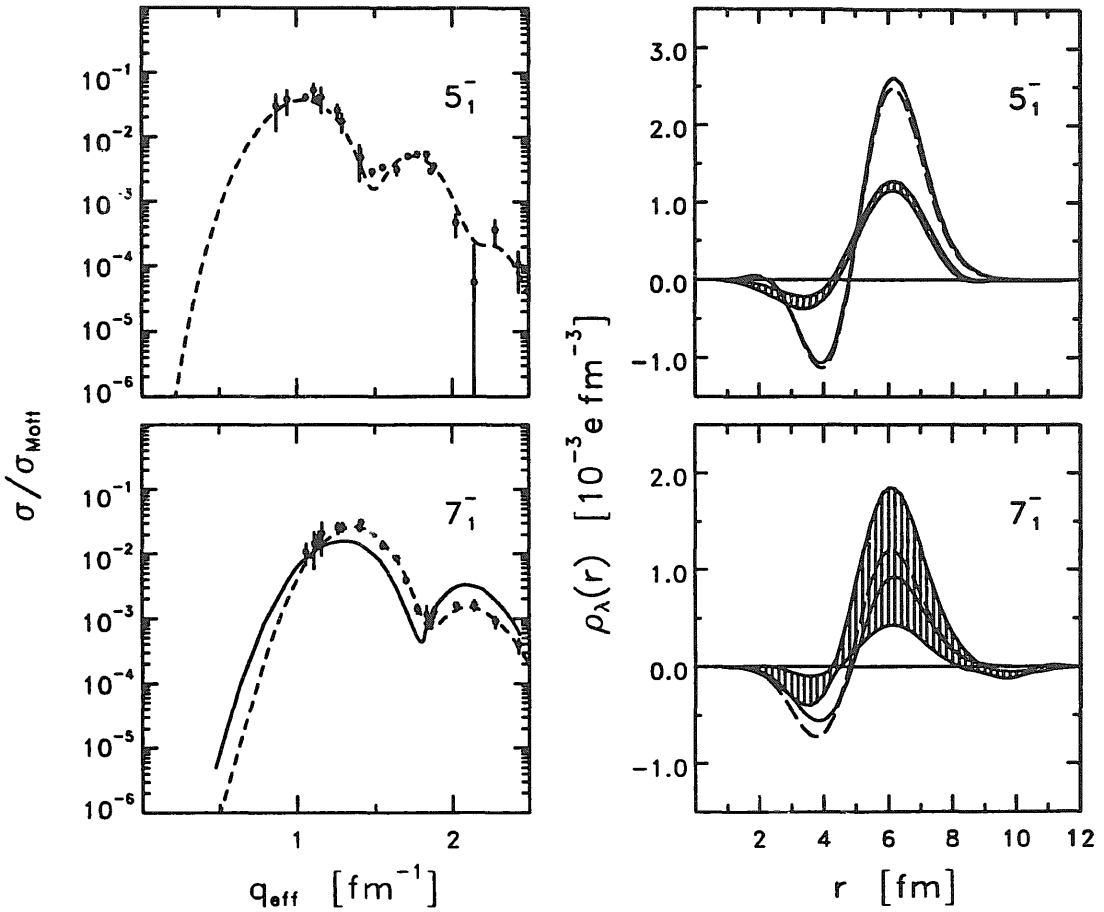

Fig. 6. The same as fig. 3 but for the 5_1^- and 7_1^- states in ^{196}Pt. The solid curve through the data of the 7_1^- state is calculated from the transition density obtained with set I parameters.

maxima at 6.1 fm. The B(E7) value for the 7_1^- level is not well determined due to the large error bars on the transition charge density and it is not presented in table 1. According to the QPM calculation the 5_1^- state is a mixture of 48% of the first one-phonon 5^- configuration and 36% of the two-phonon $[2_1^+ \times 5_1^-]_{5^-}$ configuration; the wave function of the 7_1^- state has a 48% contribution of the first one-phonon 7^- configuration and 30% of the two-phonon $[2_1^+ \times 5_1^-]_{7^-}$ configuration. Although the shape of the experimental density of the 5_1^- state is reproduced well in this calculation, the collectivity of this state is considerably overestimated. It can be weakened by adjusting the parameter of the residual interaction $\kappa_0^{5^-}$ which was fixed in this calculation to be equal to $\kappa_0^{3^-}$, but this will lead to an unrealistically small value of this parameter. Because of the large experimental uncertainties in the transition charge density of the 7_1^- state, the form factor calculated for the transition density predicted for this state is also compared to the experimental data (see fig. 6). The agreement is quite reasonable.

In general, microscopic calculations based on a spherical mean-field approach reproduce reasonably well the set of data from the present experiment. From similar experimental data in the transitional nucleus ^{146}Nd it was concluded that ^{146}Nd is

a nucleus with a shape coexistence of prolate-deformed and spherically symmetric shapes in which the lowest excited states are characterized by the deformation of the ground state while the higher excitations can be considered as vibrational ones [6]). Here we may conclude that all low-lying states in ^{196}Pt can be treated as excitations of a spherical nucleus but the structure of all of these states appears to be rather complicated.

5. Summary and conclusions

The form factors of the ground state and nine low-lying collective levels in ^{196}Pt have been measured in a $q_{\rm eff}$ range 0.36–2.43 fm^{-1} by electron scattering. The first 2^+, three 3^-, three 4^+, one 5^- and one 7^- states have been observed. The transition charge densities of these states as well as the ground-state charge density have been deduced in Fourier–Bessel analyses of these data. The extracted transition densities peak between 5.9 and 6.5 fm, indicating the collective nature of these levels. It has been shown that a reasonably good agreement can be achieved in a microscopic treatment of the low-lying states of the triaxial ^{196}Pt nucleus based on spherical mean-field calculations. The single-particle basis for such calculations was taken from the self-consistent FFS theory which proved to give good agreement with experimental data for the ground-state charge densities. Unfortunately, the present realization of this approach does not take into account the admixture of complex configurations to one-phonon states (this work is still in progress), and only the transition charge density of the 2_1^+ state was calculated. The full analysis for other states has been performed in terms of phonon excitations within the QPM which consistently takes into account the interplay between phonon configurations of different complexity. The structure of most of the low-lying states in ^{196}Pt appears to be rather complicated in this picture with the strength of the first collective one-phonon configurations for each λ^π fragmented over several low-lying states. Since the shape of the transition densities of low-lying states with large $B(E\lambda)$ values is determined mainly by this collective one-phonon configuration, this results in the appearance of several low-lying states with transition charge densities that are very similar to each other. This feature has been observed in the present experiment and the transition densities of three 4^+ states and at least two 3^- states displaying such a behaviour have been extracted. Although the transition densities of these states are rather similar, the positions of their surface maxima vary from one state to another. This is explained by the microscopic QPM calculation to be a result of the admixture of two-phonon configurations. Although the size of the shift of the maximum is underestimated by the calculation for some states, the sign of the shift is always predicted correctly. It should be remarked that the results obtained in the QPM with set II especially adjusted for ^{196}Pt give hardly any improvement over the results obtained with the global set I. This indicates that in general it may suffice to use set I in calculations of this kind.

One of us (V.Yu.P.) thanks the Nuclear Physics Groups of the Free University of Amsterdam, the NIKHEF and the KVI for the hospitality during his stay in the Netherlands. This work is part of the research program of the National Institute for Nuclear Physics and High-Energy Physics (NIKHEF-K) and the Foundation for Fundamental Research of Matter (FOM), which is financially supported by the Netherlands Organisation for Scientific Research (NWO).

References

1) O. Schwentker, J. Dawson, J. Robb, J. Heisenberg, J. Lichtenstadt, C.N. Papanicolas, J. Wise, J.S. McCarthy, L.T. van der Bijl and H.P. Blok, Phys. Rev. Lett. **50** (1983) 15
2) W. Kim, J.P. Connelly, J.H. Heisenberg, F.W. Hersman, T.E. Milliman, J.E. Wise, C.N. Papanicolas, S.A. Fayans and A.P. Platonov, Phys. Rev. C, to be published
3) J.E. Wise, J.P. Connelly, F.W. Hersman, J.H. Heisenberg, W. Kim, M. Leuschner, S.A. Fayans, A.P. Platonov, E.E. Saperstein and V.Yu. Ponomarev, Phys. Rev. **C45** (1992) 2701
4) R.K.J. Sandor, H.P. Blok, U. Garg, M.N. Harakeh, C.W. de Jager, V.Yu. Ponomarev, A.I. Vdovin and H. de Vries, Phys. Lett. **B233** (1989) 54
5) R.K.J. Sandor, H.P. Blok, U. Garg, M.N. Harakeh, C.W. de Jager, V.Yu. Ponomarev, A.I. Vdovin and H. de Vries, Nucl. Phys. **A535** (1991) 669
6) R.K.J. Sandor, H.P. Blok, M. Girod, M.N. Harakeh, C.W. de Jager, V.Yu. Ponomarev and H. de Vries, Nucl. Phys. A, submitted
7) R.K.J. Sandor, H.P. Blok, U. Garg, M. Girod, M.N. Harakeh, C.W. de Jager and H. de Vries, Phys. Rev. **C43** (1991) R2040
8) R.K.J. Sandor, H.P. Blok, M. Girod, M.N. Harakeh, C.W. de Jager and H. de Vries, Nucl. Phys. A, submitted
9) R.K.J. Sandor, Ph.D. thesis, Free University, Amsterdam (1991), unpublished
10) W. Kim, J.R. Calarco, J.P. Connelly, J.H. Heisenberg, F.W. Hersman, T.E. Milliman, J.E. Wise, B.L. Miller, C.N. Papanicolas, V.Yu. Ponomarev, E.E. Saperstein and A.P. Platonov, Phys. Rev. **C44** (1991) 2400
11) W. Kim, B.L. Miller, J.R. Calarco, L.S. Cardman, J.P. Connelly, S.A. Fayans, B. Frois, D. Goutte, J.H. Heisenberg, F.W. Hersman, V. Meot, T.E. Milliman, P. Mueller, C.N. Papanicolas, A.P. Platonov, V.Yu. Ponomarev and J.E. Wise, Phys. Rev. **C45** (1992) 2290
12) X.H. Phan, H.G. Andresen, L.S. Cardman, J.M. Cavedon, J.C. Clemens, B. Frois, M. Girod, D. Gogny, D. Goutte, G. Grammaticos, R. Hofmann, M. Huet, P. Leconte, S.K. Platchkov, I. Sick and S.E. Williamson, Phys. Rev. **C38** (1988) 1173
13) W. Boeglin, P. Egelhof, I. Sick, J.M. Cavedon, B. Frois, D. Goutte, V. Meot, P. Leconte, X.H. Phan, S.K. Platchkov, S. Williamson and M. Girod, Nucl. Phys. **A477** (1988) 399
14) C.N. Papanicolas, J. Heisenberg, J. Lichtenstadt, J.S. McCarthy, D. Goutte, J.M. Cavedon, B. Frois, M. Huet, P. Leconte and I. Sick, Phys. Rev. Lett. **52** (1984) 247
15) W.T.A. Borghols, N. Blasi, R. Bijker, M.N. Harakeh, C.W. de Jager, J.B. van der Laan, H. de Vries and S.Y. van der Werf, Phys. Lett. **B152** (1985) 330
16) V.G. Soloviev, Theory of complex nuclei (Pergamon, Oxford, 1976)
17) A.I. Vdovin and V.G. Soloviev, Sov. J. Part. Nucl. **14** (1983) 99
18) V.V. Voronov and V.G. Soloviev, Sov. J. Part. Nucl. **14** (1983) 583
19) V.G. Soloviev, Prog. Part. Nucl. Phys. **17** (1987) 107
20) S.A. Fayans, V.A. Khodel and E.E. Saperstein, Nucl. Phys. **A317** (1979) 424
21) A.P. Platonov and E.E. Saperstein, Nucl. Phys. **A486** (1988) 63
22) A.V. Smirnov, S.V. Tolokonnikov and S.A. Fayans, Sov. J. Nucl. Phys. **48** (1988) 995
23) P.T. Deason, C.H. King, R.M. Ronningen, T.L. Khoo, F.M. Bernthal and J.A. Nolen Jr., Phys. Rev. **C23** (1981) 1414
24) F.T. Baker, A. Scott, T.H. Kruse, W Hartwig, E. Ventura and W. Savin, Nucl. Phys. **A266** (1976) 337
25) N. Blasi, M.N. Harakeh, W. A. Sterrenburg and S.Y. Van der Werf, Phys. Rev. **C31** (1985) 653

26) N. Blasi, Ph.D. thesis, Rijksuniversiteit Groningen, Groningen (1984), unpublished
27) J.A. Cizewski, E. R. Flynn, R.E. Brown, D.L. Hanson, S.D. Orbesen and J.W. Sunier, Phys. Rev. C23 (1981) 1453
28) J.A. Cizewski, R.F. Casten, G.J. Smith, M.R. Macphail, M.L. Stelts, W.R. Kane, H.G. Börner and W.F. Davidson, Nucl. Phys. A323 (1979) 349
29) P. Schüler, T. Recht, H. Wilzek, K. Hardt, C. Günther, K.P. Blume, K. Euler and V. Kölschbach, Z. Phys. A317 (1984) 313
30) A. Mauthofer, K. Stelzer, J. Idzko, Th.W. Elze, H.J. Wollersheim, H. Emling, P. Funhs, E. Grosse and D. Schwalm, Z. Phys. A336 (1990) 263
31) C. de Vries, C.W. de Jager, L. Lapikás, G. Luijckx, R. Maas, H. de Vries and P.K.A. de Witt Huberts, Nucl. Instr. Meth. A233 (1984) 1
32) C.E. Hyde-Wright, Ph.D. thesis, MIT (1984), unpublished
33) K. Merle, Ph.D. thesis, University of Mainz, Mainz, Germany (1976), unpublished
34) J. Heisenberg, Adv. Nucl. Phys. 12 (1981) 61
35) S.A. Fayans, to be published
36) C. Bernhardt, Diplomarbeit, University of Mainz, Mainz, Germany (1990), unpublished
37) J. Halperin, Nucl. Data Sheets 24 (1979) 485